Tuning the ultralow β^* optics at the KEK Accelerator Test Facility 2

R. Yang,[1,*] A. Pastushenko,[1,2] A. Aryshev,[3,4] M. Bergamaschi,[1] V. Cilento,[1,2] A. Faus-Golfe,[2] M. Fukuda,[3,4] P. Korysko,[1] K. Kubo,[3,4] S. Kuroda,[3,4] T. Naito,[3,4] T. Okugi,[3,4] F. Plassard,[1,†] N. Terunuma,[3,4] and R. Tomás[1]

[1]*European Organization for Nuclear Research, Geneva CH-1211, Switzerland*
[2]*IJCLab, CNRS/IN2P3, Université Paris-Saclay, Orsay 91898, France*
[3]*High Energy Accelerator Research Organization (KEK), Tsukuba, Ibaraki 350-0801, Japan*
[4]*School of High Energy Accelerator Science, SOKENDAI, Tsukuba, Ibaraki 350-0801, Japan*

(Received 25 May 2020; accepted 8 July 2020; published 23 July 2020)

For future linear colliders, a nanometer-scale beam size at the interaction point (IP) is one of the most challenging technical aspects. To explore the feasibility of a final focus system with a high chromaticity level, comparable to that of the Compact Linear Collider, the ultralow β^* optics has been proposed and tuned at the KEK Accelerator Test Facility 2. In this paper, the recent experimental results are presented, which demonstrate the capability of achieving and stabilizing a vertical average beam size of 60 nm and below at the virtual IP. The observed vertical beam size is about 20 nm above the numerical predictions in the presence of static and dynamic imperfections. We interpret this discrepancy as beam size growth due to multipole fields, beam jitters and wakefield effects, and diagnostic errors.

DOI: 10.1103/PhysRevAccelBeams.23.071003

I. INTRODUCTION

A nanometer-scale beam size at the interaction point is a fundamental ingredient to achieve the design luminosity in future energy-frontier linear colliders. To demagnify the beam to the required spot sizes, a novel local chromaticity correction-based final focus system has been proposed and considered for the baseline designs of the International Linear Collider (ILC) and Compact Linear Collider (CLIC) [1–6]. To address the practical feasibility of this new scheme envisioned for future linear colliders, the Accelerator Test Facility 2 (ATF2) project has been launched at KEK, aiming to achieve a nanometer beam size and provide nanometer beam stability at the virtual interaction point (IP) [7–10]. The nominal optics ($\beta_x^* = 4$ mm, $\beta_y^* = 0.1$ mm) implemented at ATF2 closely resembles the ILC final focus system (FFS) in terms of requirements, with a goal beam size of 37 nm. To reduce the impact of magnetic multipole errors, the so-called 10×1 optics with a 10 times larger IP horizontal β function than the original design has been used for the recent beam operations. To explore the feasibility of a FFS with a higher chromaticity, comparable to that of the CLIC FFS, the ultralow β^* optics has been proposed that has a 4 times smaller IP vertical β function than the nominal and a target vertical beam size of 23 nm [11–16]. The ultralow β^* optics intends to explore the uncharted chromatic territory and push the limits of ATF2.

The complexity of the FFS tuning is proportional to the magnitude of the chromaticity. Tuning both the 10×1 optics and the ultralow β^* optics in the presence of realistic imperfections is of great difficulty, but the latter is much more challenging. In the 10×1 optics, a capability for

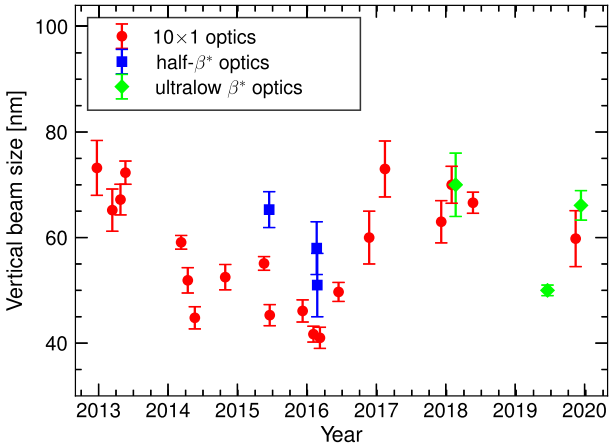

FIG. 1. The minimum IP vertical beam sizes obtained in every operation period from 2012 to 2020. For comparison sake, the results achieved in the IPBSM 174° mode with stable modulation depths of more than 0.2 are shown.

*renjun.yang@cern.ch
†Present address: Brookhaven National Laboratory, Upton, New York, USA.

TABLE I. ATF main parameters [24–26].

Beam energy [GeV]	1.3
Bunch charge [nC]	0.16–1.6
Vertical emittance [pm]	>4
Horizontal emittance [nm]	1.2
Energy spread [%]	0.056 (0.08)[a]
Bunch length [mm]	5.3 (7)[a]
Number of bunches	1–20
Repetition rate [Hz]	3.12

[a]For a bunch charge of 1.6 nC.

repeatable tuning of a vertical beam size of less than 60 nm has been successfully demonstrated, as shown in Fig. 1. A record beam size of 41.1 ± 0.7 nm has been achieved with fast orbit stabilization in two-bunch mode in 2016 [17]. Before tackling the ultralow β^* optics tuning, the half-β^* optics ($\beta_x^* = 40/100$ mm, $\beta_y^* = 0.05$ mm) has been studied to uncover the plausible limits for beam tuning with a higher chromaticity, and a vertical beam size of 51 ± 6 nm has been obtained [15]. However, such small beam sizes are hardly reproduced after, due to a reduction of devoted machine time, degradation of the IP beam size monitor (IPBSM) performance, and unstable beam conditions (unexpected horizontal orbit oscillation). Nevertheless, small beam size tuning in the ultralow β^* optics has been carried out with an optimized IP horizontal β function of 100 mm.

In this paper, the feasibility of the ultralow β^* optics has been first verified through tuning simulations, followed by experimental demonstrations. Moreover, the possible limits for the nanometer beam size achievement are discussed, as well as some mitigation measures.

II. ATF2 BEAM LINE

ATF2 is an extended extraction line to the ATF damping ring (DR), which supplies a high-quality electron beam with a vertical normalized emittance of about 30 nm, comparable to the requirement of the ILC beam delivery system. The major beam parameters for the extracted beam are summarized in Table I. The ATF2 beam line contains three sections: the extraction line (EXT) for the beam extraction and manipulation, the matching section for the adjustment of the downstream optics, and the FFS (see Fig. 2). The EXT section comprises a "dogleg" inflector with two skew quadrupoles adjacent to the two 10° bends

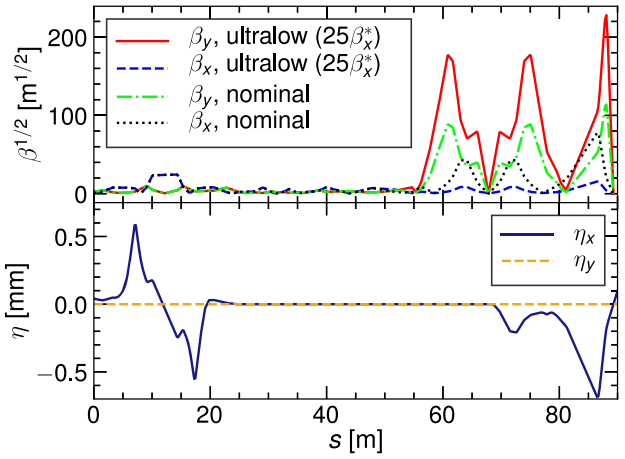

FIG. 3. β function and dispersion (η) along the ATF2 beam line for the ultralow β^* ($25\beta_x^*$) and nominal optics.

for the vertical dispersion and xy-coupling corrections, an ILC-style coupling correction system consisting of four skew quadrupoles, and four optical transition radiation (multi-OTR) monitors providing fast diagnostics of emittances and Twiss parameters [18,19]. Besides, an intratrain beam position feedback system (FONT) has been deployed in the EXT line for fast beam stabilization in the vertical plane [20,21]. Six bipolar quadrupoles in the matching section are for the optics matching between the EXT section and the FFS. The FFS compensates the chromaticity locally using two sextupoles adjacent to the final doublet (FD) with nonzero horizontal dispersion generated by upstream bends. Another three sextupoles are placed upstream of the FD in proper phase with the FD sextupoles to cancel the higher-order aberrations. To loosen the tolerance on magnet multipole errors, a group of skew sextupoles has been installed in the FFS [22]. Furthermore, two octupoles have been introduced to correct the residual third-order aberrations. Moreover, a wakefield compensation setup, that contains bellows and a C-band pillbox on a mover, has been installed in the large β_y region to diminish the downstream beam distortions [23]. Currently, there are 21 strip line beam position monitors (BPMs) and 15 C-band cavity BPMs distributed in the EXT line and downstream, respectively. The various optics for the ATF2 beam line are depicted in Fig. 3, and the FFS parameters for ATF2, ILC, and CLIC are summarized in Table II.

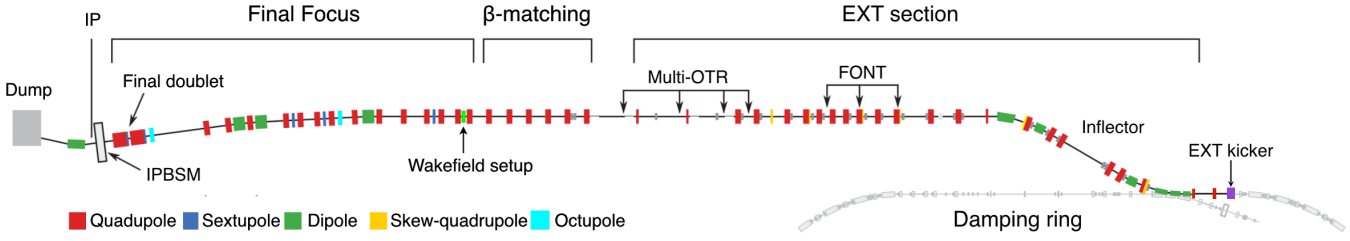

FIG. 2. Schematic layout of the ATF2 beam line.

TABLE II. The major FFS parameters for ATF2, in comparison with the ILC and CLIC baseline designs [1,2,6]. L^* is the distance between the last quadrupole and IP, ξ_y the vertical chromaticity, ε_y the vertical emittance, σ_E the energy spread, and σ_y^* the IP vertical beam size.

	ATF2 nominal	ATF2 half-β^*	ATF2 ultralow β^*	ILC (500 GeV)	CLIC (3 TeV)
L^* [m]	1	1	1	(3.5/4.5)[a]	6
β_x^* [mm]	4 (40)[b]	4 (100)[c]	4 (100)[c]	11	7
β_y^* [mm]	0.1	0.05	0.025	0.48	0.12
$\xi_y \sim L^*/\beta_y^*$	10000	20000	40000	(7300/9400)[a]	50000
ε_y [pm.rad]	12	12	12	0.07	0.003
σ_E [%]	0.8	0.8	0.8	(0.07/0.12)[d]	0.3
$\sigma^*_{y,\mathrm{design}}$ [nm]	37	25	23	5.9	0.9
$\sigma^*_{y,\mathrm{measured}}$ [nm]	42.3 ± 2.7[b]/41.1 ± 0.7[b,e]	51 ± 6[c]	50.1 ± 0.6[c]	⋯	⋯

[a]SiD/ILD detector configurations.
[b]Optics with loosened β_x, $10\beta_x^*$.
[c]Optics with loosened β_x, $25\beta_x^*$.
[d]Positron or electron beam of ILC.
[e]Results achieved with beam stabilization in two-bunch mode.

For the nanometer beam size diagnostic at the IP, a laser-interferometer beam size monitor has been built at ATF2. Two paths of laser are focused at the IP to form a vertically oriented interference fringe pattern, the phase of which could be scanned by adjusting the length of one incident laser path. The vertical beam size is then inferred from the modulation depth in the rate of the Compton scattering photons collected by a downstream CsI or Cherenkov calorimeter-type detector, which can be expressed as [27–32]

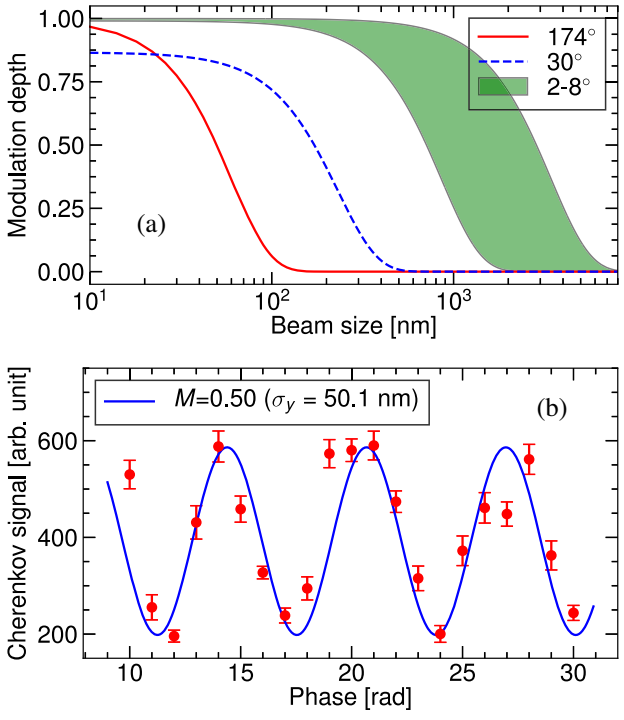

FIG. 4. IPBSM modulation depth as a function of the beam size for each collision mode (a) and an example vertical beam size measurement in the 174° mode (b). Here, a unity modulation reduction factor has been assumed.

$$\sigma_y = \frac{d}{2\pi}\sqrt{2\log\left(\frac{C|\cos\theta|}{M}\right)} \tag{1}$$

with

$$d = \frac{\lambda}{2\sin(\theta/2)}, \tag{2}$$

where d is the fringe pitch, θ the crossing angle of two laser paths, C the modulation reduction factor, M the modulation depth, and λ the laser wavelength. Three crossing angles, 2°–8°, 30°, and 174°, are designed to cover a beam size from a few micrometers to about 20 nm; see Fig. 4(a). The collision mode can be automatically switched to allow a continuous beam tuning. Besides, remote optimization of the fringe pattern is available for acquiring the sharpest fringe contrast, i.e., a maximum modulation depth. An example modulation scan in the 174° mode is shown in Fig. 4(b).

III. TUNING SIMULATION

To evaluate the tuning performance of the designed optics, Monte Carlo simulations have been performed incorporating the measured multipolar errors and static and dynamic machine errors. The static errors considered in the simulation are summarized in Table III. The dynamic errors mainly include beam jitters at the extraction, mechanical vibration of the FD quadrupoles, and the ground motion (GM). We assumed that the position and angular jitters at the extraction are 10% of beam sizes, while they might occasionally rise to 30% due to a poor DR or extraction commissioning [33,34]. The mechanical vibrations of 5.1 and 10 nm are assumed for the FD quadrupoles, QD0 and QF1, respectively. The former is from the previous vibration measurements, and the latter is 1.5 times the measured value (6.5 nm), since the QF1 magnet has been replaced after the measurements [8,35].

TABLE III. Major static machine errors considered for the tuning simulations [9,22].

Error	Element	σ_{err}
Misalignment [μm]	Dipole/quad./sext./BPM	100
Rolling error [μrad]	Dipole/quad./sext.	200
Strength error [%]	Dipole/quad. (EXT)/sext.	0.1
	Quadrupole (FFS)	0.001
Mover accuracy [nm]	FFS quad./sext.	100
BPM resolution [μm]	Strip line BPM	5
	C-band cavity BPM	0.2
BPM scaling error [%]		1
BBA accuracy [μm]	FFS dipole/quad./sext.	100

The ground motion is implemented on a bunch-by-bunch basis using a two-dimensional (2D) GM generator based upon the earlier measurements at the site [36,37]. The ground motion is governed by traveling-wave-like fast motion and slow motion for a timescale of [0.02, 10] and $[10, 10^5]$ s, respectively. In the vertical plane, the wavelike motion is given by [38,39]

$$\Delta y(t,s) = \sum_i \sum_j a(w_i,k_j)\cos(-w_i t + k_j s + \phi_{ij}) \tag{3}$$

with

$$a^2(w_i,k_j) = \frac{2}{\pi^2}\int_{w_i}^{w_{i+1}}\int_{k_j}^{k_{j+1}} P(w,k)dkdw, \tag{4}$$

where $a(w_i,k_j)$ represents the oscillation amplitude around angular frequency w_i and wave number k_j, s the longitudinal location, t the time, ϕ_{ij} a random phase, and $P(w,k)$ the 2D power spectrum density (PSD), given by

$$P(w,k) = \sum_m \frac{a_m U_m}{1+\left(\frac{d_m(w-w_m)}{w_m}\right)^4} \tag{5}$$

with

$$U_m = \begin{cases} \frac{2}{\sqrt{k_m^2-k^2}} & |k| \le k_l, \\ 0 & |k| > k_l, \end{cases} \tag{6}$$

where a_m, d_m, w_m, and k_m are the amplitude, width, frequency, and wave number of peaks in the spectrum, respectively. The 2D power spectrum could not be measured directly, and these parameters are determined through the related one-dimensional PSD (see Fig. 5). The slow GM is described by the "*ATL*" law, where A is a constant assumed as $(27\pm3)\times10^{-6}$ $\mu\mathrm{m}^2/(\mathrm{ms})$ that measured inside the KEKB 12-meter deep tunnel and T is set as 15 min (time for one tuning knob scan) [40].

The tuning simulation is performed through a script developed in SAD [41], a program used for online optics modeling and correction at ATF. To acquire sufficient statistics, at least 100 machines are used for every tuning study. For each machine, the machine errors are randomly initialized following Gaussian distribution of σ_{err}. A Gaussian fit to the projected core distribution gives the beam size. The multishot beam size ($\sigma_{y,\mathrm{m}}$) is defined by fitting the particle distribution accumulated over at least 30 bunches with a time interval of 5 s.

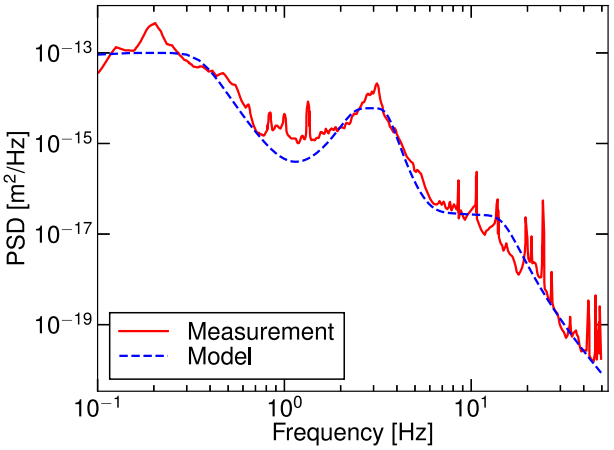

FIG. 5. Measurement and modeling of the ground motion PSD function at ATF2 [36].

For comparison sake, we simulated three optics: the ultralow β^* optics, the 10×1 optics, and the nominal optics using the beam parameter summarized in Table I. The implemented tuning process mimics that for the experiments, as follows: global orbit correction using one-to-one and singular value decomposition techniques with the FFS sextupoles power off, IP β-function matching with a 5% uncertainty, fine orbit correction reducing the FFS orbit to less than 300 μm, global dispersion and coupling correction using the skew quadrupoles in the EXT section, beam-based alignment (BBA) of the sextupoles, skew sextupoles, and FD quadrupoles, and then iterative optimizations of the IP vertical beam size using dedicated linear and nonlinear tuning knobs with the FFS sextupoles power on. Typically, a few iterations of these tuning knobs are sufficient to reduce the IP spot size near the design value [22].

Adapting the described tuning procedure, the vertical single-shot beam sizes (σ_{y0}) are gradually reduced to 32.2 ± 4.5, 38.8 ± 2.8, and 40.9 ± 3.3 nm for the ultralow β^*, 10×1, and nominal optics, respectively, as shown in Fig. 6. For the ultralow β^* optics, the vertical beam size converges to less than 100 nm after the first iteration of linear aberration corrections and finally reaches ~32 nm after another few iterations of linear and nonlinear knob corrections. Besides, a vertical beam size of less than 30 nm is obtained in a probability of 0.4. The remaining discrepancy between the simulated and betatron beam sizes is mainly owing to the residual third-order aberrations, which require further corrections using the octupoles [13,42].

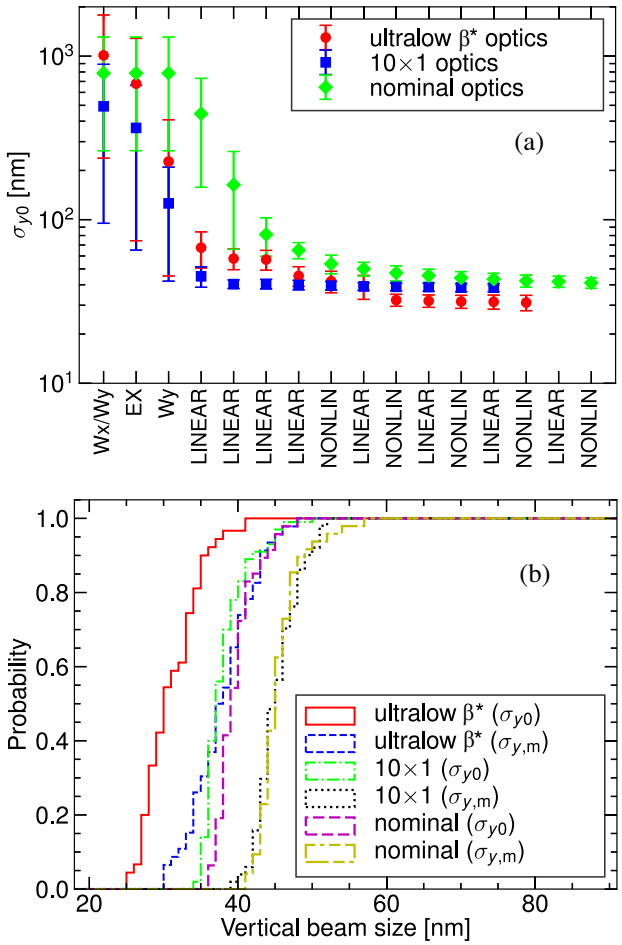

FIG. 6. Vertical beam size throughout the tuning procedure (a) and cumulative histogram of the final single-shot and multishot beam sizes (b). The horizontal labels in (a) are Wx and Wy, the horizontal and vertical beam waist adjustments, respectively, using the FD quadrupoles; EX, the IP horizontal dispersion correction; LINEAR, correction of the vertical waist, dispersion, and coupling from horizontal momentum employing linear knobs; and NONLIN, correction of residual chromaticity and second-order aberrations by applying nonlinear knobs.

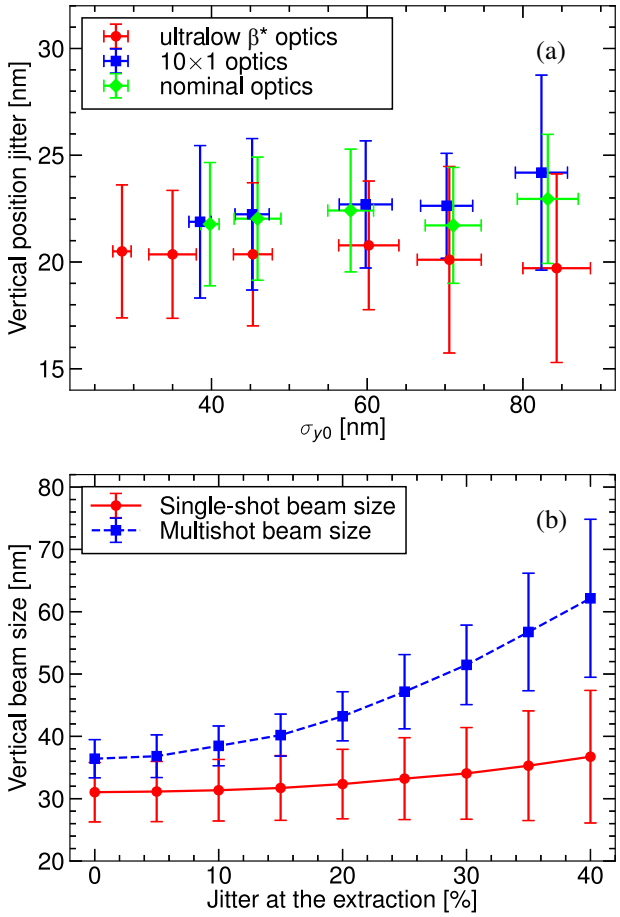

FIG. 7. IP vertical position jitter versus the single-shot beam size (a) and vertical beam size growth as a function of the initial beam jitter at the extraction for the ultralow β^* optics (b).

Incorporating the dynamic errors, the vertical multishot beam sizes ($\sigma_{y,m}$) increase to 38.3 ± 3.8, 44.9 ± 2.4, and 46.4 ± 2.9 nm, for the ultralow β^*, 10×1, and nominal optics, respectively, due to notable IP vertical position jitters, as shown in Fig. 6(b). The vertical beam sizes predicted by tuning simulations are summarized in Table IV.

TABLE IV. Vertical beam size obtained through tuning simulations. $\sigma_{y,\beta}$, σ_{y0}, and $\sigma_{y,m}$ are betatron, single-shot, and multishot beam sizes, respectively.

Optics	$\sigma_{y,\beta}$ [nm]	σ_{y0} [nm]	$\sigma_{y,m}$ [nm]
Ultralow β^*	17.3	32.2 ± 4.5	38.3 ± 3.8
10×1	34.6	38.8 ± 2.8	44.9 ± 2.4
Nominal	34.6	40.9 ± 3.3	46.4 ± 2.9

The induced IP vertical position jitters are 20.8 ± 3.4, 22.6 ± 3.0, and 22.0 ± 3.3 nm for the ultralow β^*, 10×1, and nominal optics, respectively, considering all dynamic errors. Moreover, the vertical position jitter tends to be constant when reducing the beam size below 100 nm, where the vertical waist shift is negligible, as shown in Fig. 7(a). Contributions from the fast ground motion and the vibration are about 15 and 11 nm, respectively. They are similar for the three different optics owing to the same transfer matrix from the FFS magnets to the IP. The IP vertical position jitters propagated from the extraction point are about 10 and 13 nm for the ultralow β^* and 10×1 optics, respectively. For a stable beam orbit in the EXT section, the residual IP vertical position jitter is about 18 nm, a probable lower limit that could be obtained with the currently available beam stabilization setups. On the other hand, the actual beam jitter at the extraction may fluctuate wildly depending on the beam extraction and DR conditions. Assuming the initial beam jitters of 30% of beam sizes, the multishot beam size increases to 51.5 ± 6.4 nm due to IP position jitter for the ultralow β^* optics, as shown in Fig. 7(b). The IP vertical position jitters from

TABLE V. IP vertical position jitter induced by various dynamic errors. $\sigma_{\Delta y,g}$ and $\sigma_{\Delta y,v}$ are the position jitters due to fast GM and FD-quadrupoles vibration, respectively, while $\sigma_{\Delta y,gv}$ is the position jitter produced by fast GM plus FD-quadrupoles vibration. $\sigma_{\Delta y}$ is the position jitter from fast GM, FD-quadrupoles vibration and 10% initial beam jitters.

Optics	$\sigma_{\Delta y,g}$ [nm]	$\sigma_{\Delta y,v}$ [nm]	$\sigma_{\Delta y,gv}$ [nm]	$\sigma_{\Delta y}$ [nm]
Ultralow β^*	14.8 ± 2.5	11.7 ± 1.4	17.9 ± 3.0	20.8 ± 3.4
10×1	14.8 ± 2.4	11.5 ± 2.1	17.8 ± 2.9	22.6 ± 3.0
Nominal	15.7 ± 2.5	10.2 ± 2.1	18.0 ± 3.1	22.0 ± 3.3

various error sources are summarized in Table V. Besides, an IP horizontal position jitter about 10% of the horizontal beam size is also indicated, which is tightly correlated to the initial jitter level at the extraction.

IV. EXPERIMENTS

Experimental studies of the ultralow β^* optics ($25\beta_x^*$) have been conducted since 2017. The IP vertical beam size was gradually reduced along with improved machine conditions, and we achieved a stable beam size of 60 nm and below in June 2019 following the tuning procedure described after.

In general, ATF2 tuning mainly consists of EXT tuning, optics matching, and FFS tuning. First of all, the incoming beam is steered manually to deliver beam to the dump, followed by cavity-BPM calibrations. The horizontal and vertical dispersion are corrected using a pair of quadrupoles (QF1X and QF6X) and the paired skew quadrupoles (QS1X and QS2X in the same polarity) located in the dispersive region, respectively. Besides, the vertical dispersion near the extraction is suppressed by introducing a local orbit bump in the DR, if necessary. The xy coupling along the EXT section is corrected using the same paired skew quadrupoles (in the opposite polarity) and the other four skew quadrupoles. In this stage, the vertical dispersion and xy coupling in the multi-OTR region are minimized for accurate measurement of projected emittances and Twiss parameters. Regarding the measured Twiss parameters, the FFS optics is calculated and matched to the design. The IP β functions are then confirmed with the FD quadrupole scan, and we rematch the FFS optics if the difference exceeds 10% of the design values.

The FFS tuning starts with careful orbit correction to minimize the readout at the FFS BPMs to below 300 μm, as shown in Fig. 8. Then, the beam-based alignment of the sextupoles and skew sextupoles is performed. For the skew sextupoles which are not mounted on the automatic mover, we adjust the magnet manually in the tunnel to the magnetic center determined by the local orbit bump. Prior to the IP beam size tuning, the FFS vertical dispersion is carefully corrected, and the FFS orbit feedback is activated to stabilize the beam against slow drifts. Typically, the

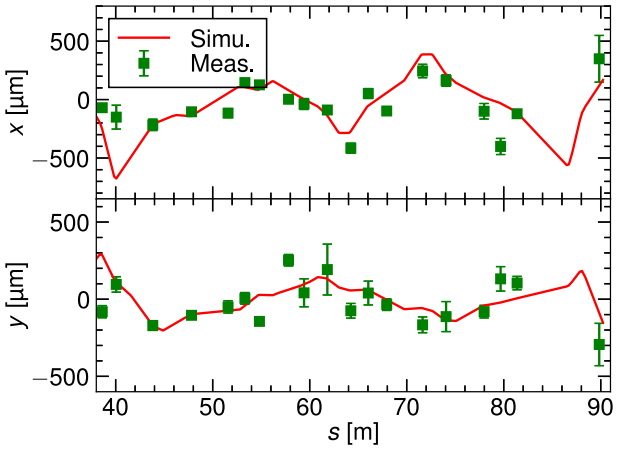

FIG. 8. The corrected FFS orbit for the June 2019 operation.

residual vertical dispersion is within 10 mm everywhere in the FFS, as shown in Fig. 9. Regarding the first-order aberrations at the IP, we first shift the betatron waist to the IP using the FD quadrupoles. If the IP horizontal dispersion is more than 1 mm, alternatively, we first minimize it using QF1 and then move the horizontal waist to the IP using the corresponding tuning knobs. A vertical beam size of less than 2 μm can typically be obtained after the preliminary FD-quadrupole corrections. In this stage, the vertical beam size is mainly determined by the residual vertical waist shift, vertical dispersion, and coupling from the particles' horizontal momentum. To mitigate these linear aberrations, we have constructed various orthogonal tuning knobs, named "linear knobs," by deliberate transverse displacements of the sextupoles. Implementing the linear-knob corrections, the vertical beam size could be declined to ~100 nm that is further held by the remaining chromatic terms and second-order aberrations. The nonlinear knobs, through orthogonal sets of strength change of

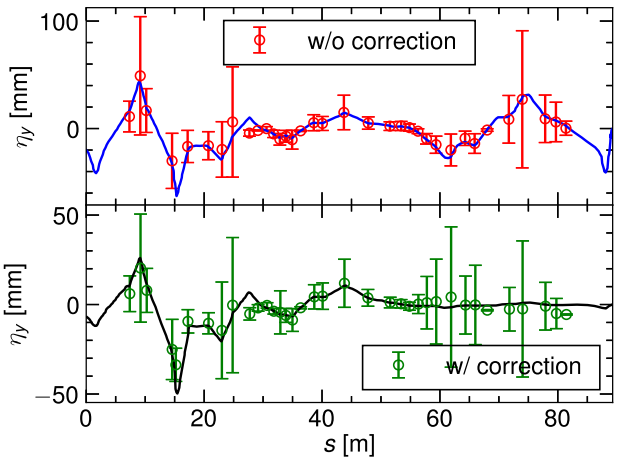

FIG. 9. Vertical dispersion correction by introducing the local orbit bump around the extraction and using the paired skew quadrupoles (QS1X and QS2X).

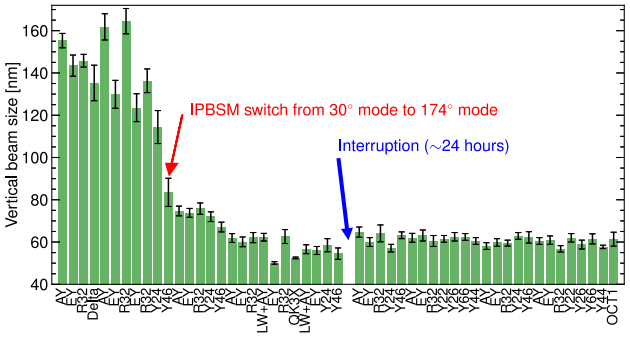

FIG. 10. IP vertical beam size versus the beam tuning in the ultralow β^* optics. The definitions of the knobs are AY, vertical waist correction; EY, vertical dispersion correction; R32, correction of coupling from horizontal momentum; Delta, xy-coupling correction; Y24, geometrical aberration correction; Y26/Y46, chromaticity corrections; Y66, second-order dispersion correction; Y22/Y44, second-order aberration corrections; LW, optimization of IPBSM laser-beam overlap; QK3X, xy-coupling correction using the QK3X skew quadrupole; and OCT1, correction using the OCT1 octupole.

the sextupoles and skew sextupoles, are then used to correct these second-order terms. To bring the vertical beam size close to the design, some iterative applications of the linear and nonlinear knobs are essential. As the most complex and time-consuming part, the IP tuning could be easily interrupted by unexpected variations of upstream conditions and minor hardware errors.

Concerning the beam tuning performed in June 2019, a vertical beam size of ∼150 nm is first observed in the IPBSM 30° mode after the first-order corrections using the FD quadrupoles and the linear knobs. With another two iterations of the first-order aberrations and chromaticity corrections, a minimum vertical beam size of 114.4 ± 7.8 nm was observed in the IPBSM 30° mode. Switching to the IPBSM 174° mode, the beam size was remeasured as 83.5 ± 6.7 nm, which indicates a modulation reduction of about 0.94 for the IPBSM 30° mode (see Sec. V for details).

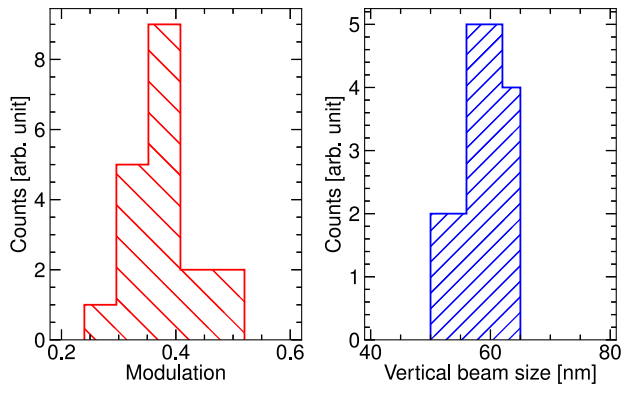

FIG. 11. Histogram of 20 consecutive measurements in the IPBSM 174° mode. The average modulation depth is 0.38 ± 0.05 that corresponds to a beam size of 59.3 ± 4.3 nm.

Executing some more iterative corrections, the IP beam size was eventually stabilized at ∼60 nm with a minimum at 50.1 ± 0.6 nm, as shown in Figs. 10 and 11. After a 24-h interruption operating in the IPBSM 30° mode, the vertical beam size was quickly recovered and maintained at ∼60 nm but not further reduced through corrections using all tuning knobs plus the octupole, leaving a gap of about 20 nm over the beam size predicted in tuning simulations.

V. DISCUSSION

The major systematic effects contributing to the 20 nm gap between the observations and the predictions have been attributed to the beam size growth due to multipolar errors, beam jitters and wakefield effects, and the IPBSM diagnostic errors. Including these systematic effects, the measured beam size ($\sigma_{y,\mathrm{IPBSM}}$) can be expressed as

$$\sigma_{y,\mathrm{IPBSM}} = \frac{1}{2k_y}\sqrt{2(2k_y^2\sigma_{y,\mathrm{m}}^2 - \sum_i \log C_i)} \tag{7}$$

with

$$\sigma_{y,\mathrm{m}}^2 = \sigma_{y0}^2 + \sigma_{\Delta y}^2 + \sigma_w^2, \tag{8}$$

where $k_y = 2\pi\sin(\theta/2)/\lambda$, $\sigma_{y,\mathrm{m}}$ the multishot beam size, σ_{y0} the single-shot beam size, $\sigma_{\Delta y}$ the beam position jitter, σ_w the beam size growth from wakefields, and C_i the modulation reduction factor. Here, beam position jitter is treated individually rather than being integrated into the modulation reduction factor as laser phase jitter. Extensive analyses have been performed to quantify the contributions from these explicit systematic effects and develop the corresponding mitigation strategies regarding the real machine conditions and preceding experiments.

A potential error source enlarging the single-shot beam size is the possible stronger multipolar fields of the FFS magnets. Assuming 5 times stronger multipoles than the previous measurements, a single-shot beam size increase from 32.2 ± 4.5 to 43.0 ± 10.6 nm is anticipated through tuning simulations, as shown in Fig. 12. Concerning a constant vertical position jitter of 20.8 ± 3.4 nm, this corresponds to a multishot beam size growth from 38.3 ± 3.8 to 47.8 ± 9.5 nm, comparable with the measurements. To verify the plausible stronger multipole components, especially for the FD quadrupoles, future beam-based measurements are required.

For a zero-charge particle beam (wakefield-free), the previous simulations in the presence of static and dynamic imperfections have indicated a considerable beam size growth owing to beam jitter. To assess the real initial beam jitters, we have measured the position jitters in the FFS and backpropagated them to the extraction based on the operational optics model. As shown in Fig. 13, the measured beam jitters in the FFS are reproduced with initial

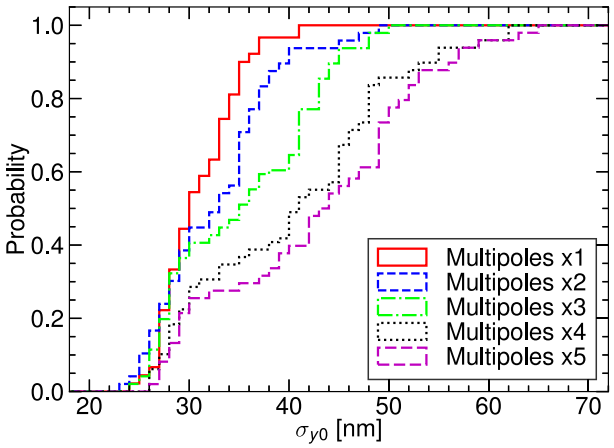

FIG. 12. Cumulative histogram of vertical single-shot beam size with stronger multipole errors.

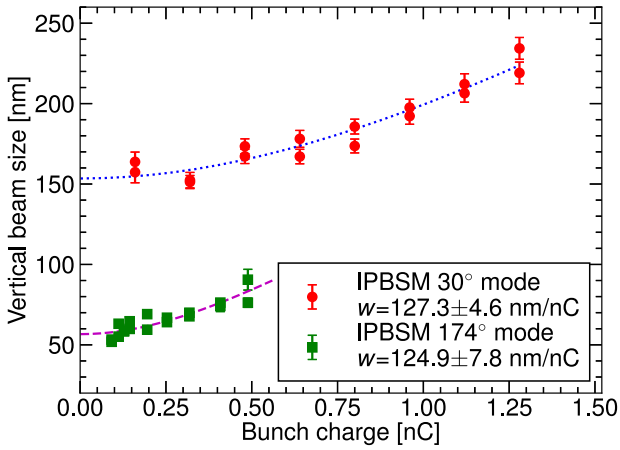

FIG. 14. Intensity dependence of the vertical beam size measured in the IPBSM 30° and 174° modes.

beam jitters of 5% of beam sizes, and, subsequently, an IP vertical position jitter of 19.2 ± 1.7 nm is deduced. To control the beam jitter along the beam line, one should carefully tune the DR and beam extraction and operate the FONT upstream feedback if necessary. For a nanometer-level stabilization at the IP, an intratrain IP feedback system and a feed-forward system for GM mitigation have been proposed and are under investigation [43,44].

Giving a bunch length of about 7 mm at a low beam energy, significant orbit and profile distortions caused by transverse wakefields have been observed at ATF2. The resulted IP beam size growth is proportional to the bunch charge, i.e., $\sigma_w = wq$, where q is the bunch charge and w has been measured as about 125 nm/nC for the ultralow β^* optics via beam intensity scans, as shown in Fig. 14. The wakefield effects have two consequences: the static component associated with a stable beam orbit and the dynamic component that depends on the amplitude of beam jitter over a well-aligned orbit. The latter is uncorrelated with the FFS optics change and can be characterized by

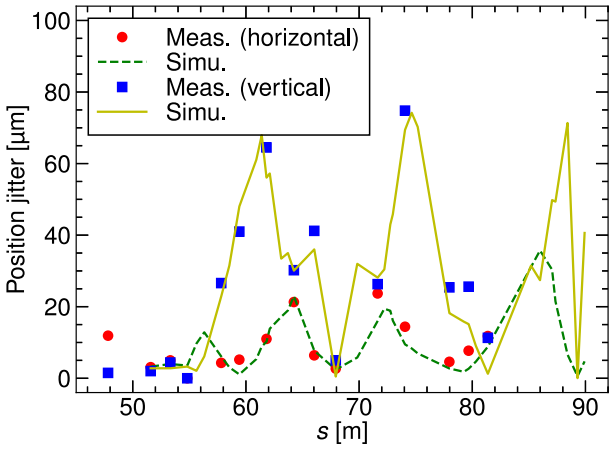

FIG. 13. Horizontal and vertical beam position jitters along the FFS. Notice that initial beam jitters of 5% of beam sizes are assumed for the simulations.

$w_d = k_d \sigma_{\Delta y'}$, where k_d is a coefficient and $\sigma_{\Delta y'}$ is the IP angular jitter denoting the position jitter in the FD phase. Some earlier measurements have indicated a coefficient k_d of 0.625 nm $(\text{nC})^{-1}$ $(\mu\text{rad})^{-1}$ [45,46]. Assuming an IP angular jitter of 180 μrad ($0.25\sigma^*_{y'}$), the static and dynamic wakefield components are evaluated to be 55 and 112.5 nm/nC, respectively, for the ultralow β^* optics. To minimize the wakefield effects, beam tuning is typically conducted at a low bunch charge (≤ 0.16 nC) and the on-mover wakefield source has to be in the optimal position [23]. Apparently, the wakefield effects can be further suppressed by beam stabilization based on fast feedback and feed-forward techniques.

The observed beam size is usually overestimated due to various systematic errors of the IPBSM, for instance, the longitudinal extent of the interference pattern, tilts between the beam and interference pattern, and variations of laser parameters and pulse-to-pulse jitters. These systematic errors tend to disrupt the laser-beam interaction and degrade the modulation depth. Following the analytical treatments established in Refs. [28–32], the probable modulation reduction is evaluated concerning the parameters and errors listed in Table VI. Moreover, the modulation reduction for the 30° mode is also assessed by

TABLE VI. Major parameters and systematic errors of the IPBSM [30–32].

Wavelength [nm]	532
Polarization [%]	>98.5
Transverse laser spot size [μm]	(23.2/19.2)[a]
Longitudinal laser spot size [μm]	(24.4/18.7)[a]
Tilt of the pattern [mrad]	0.56
Misalignment of two laser paths [%]	30[b]
Laser power imbalance [%]	20
Laser phase jitter [mrad]	240

[a]For the 30°/174° modes.
[b]Normalized to laser spot sizes.

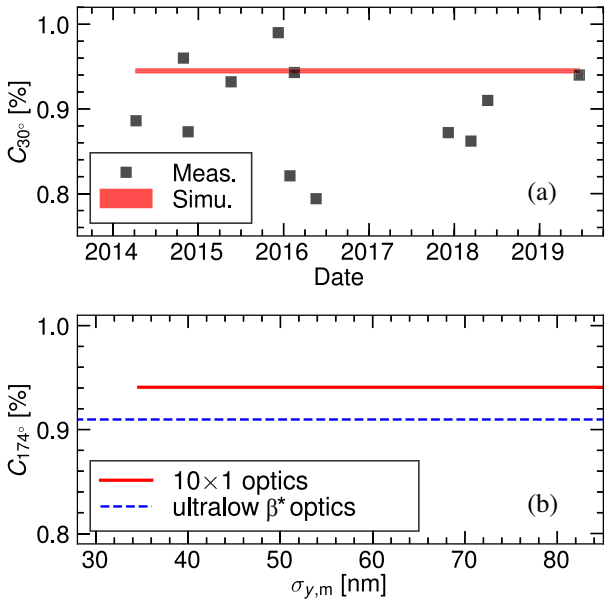

FIG. 15. Evaluations of the modulation reduction factor for the 30° mode (a) and the 174° mode (b). The height of bands in (a) represents the variance of the IP β functions.

comparing the parallel measurements in the 30° and 174° modes. The measured modulation reduction factor ranges from 0.79 to 0.99, with a couple of better cases consistent with the analytical predictions ($C \approx 0.94$), as shown in Fig. 15(a). For the 174° mode, the modulation reduction factors of 0.91 and 0.94, increasing the observed beam size by 18.4 and 14.9 nm, respectively, are predicted for the ultralow β^* and 10×1 optics, respectively, as shown in Fig. 15(b). The ultralow β^* optics presents a worse modulation reduction because of the 2 times larger IP vertical beam divergence. Here, a perfect laser spot and a stable laser-beam interaction have been supposed. However, in reality, the modulation depth may be further reduced due to an imperfect laser, fringe pattern distortions, and photon signal fluctuations.

Consequently, the single-shot beam sizes from IPBSM measurements can be evaluated, respecting the operational beam parameters. For simplicity, we approximate the IP vertical position jitter by simulations assuming 10% initial beam jitters and stable beam orbit in the EXT section with the FONT upstream feedback; see Table. V. For the ultralow β^* optics, the obtained 50.1 ± 0.6 nm beam size is found to be corresponding to a single-shot zero-current beam size of about 35.5 nm, consistent with the tuning simulations, as shown in Fig. 16(a). With a stable beam orbit in the EXT section and along the whole beam line ($\sigma_{\Delta y} \leq 10$ nm at the IP), the observed beam size might decrease to 45 and 42 nm, respectively. Furthermore, for the design beam size of 23 nm, the minimum observable beam sizes are inferred as 41.2 and 32.3 nm in the presence of the uncorrected systematic effects and orbit stabilization everywhere ($\sigma_{\Delta y} = 10$ nm, $\sigma_w = 8.8$ nm), respectively. Moreover, the

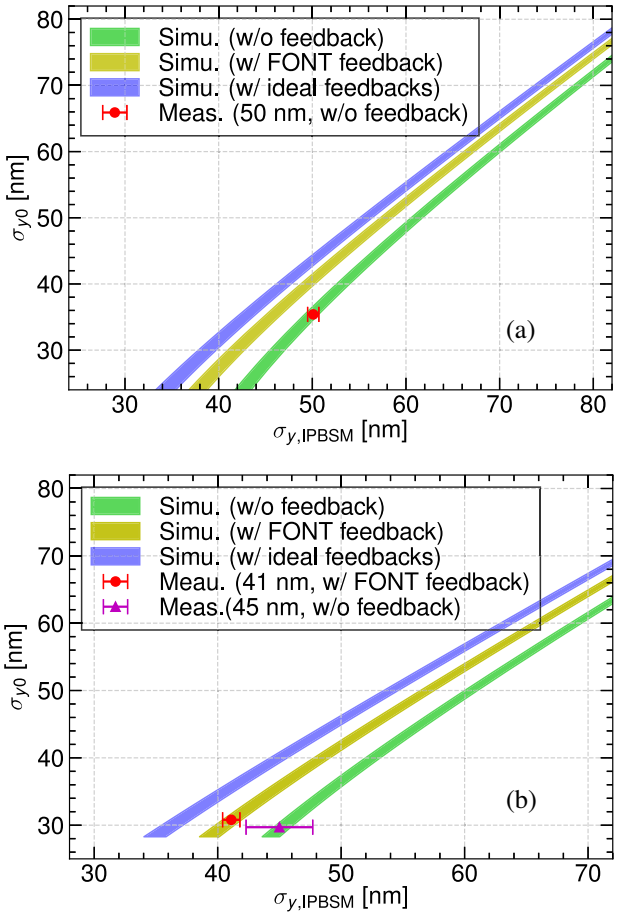

FIG. 16. Evaluation of single-shot zero-current beam sizes from IPBSM measurements for the ultralow β^* optics (a) and 10×1 optics (b). The width of the colored curves represents the uncertainty of the fringe pattern tilts referring to the electron beam.

same inference has also been implemented to the record 41.1 nm beam size achieved in the 10×1 optics thanks to the FONT upstream feedback, where the beam size was remeasured as 45.0 ± 2.7 nm without feedback. Using the measured beam parameters [$\varepsilon_y \approx 8.0$ pm and $\sigma_w \approx 17.8$ (20.3) nm for the upstream feedback on (off)], a single-shot zero-current beam size of about 30.7 nm, 8.4% larger than the betatron beam size of 28.3 nm, is predicted with satisfactory self-consistency, as illustrated in Fig. 16(b). If the beam jitter could be well controlled everywhere, the measured beam size might be decreased by another 4 nm and then be limited by the IPBSM modulation reduction.

To overcome these systematic effects and approach the design beam size, some straightforward strategies are highlighted as follows: (a) experimental verification of the multipole errors of the FFS magnets; (b) integration of the FONT upstream feedback system into the routine operation and development of advanced correction techniques to reduce beam jitter everywhere, especially at the IP; (c) automatic orbit corrections to steer beam passing through the center of both FFS magnets and high-impedance elements; (d) upgrade of the IPBSM laser and development

of a robust offline modulation-correction algorithm. Besides, continuous beam tuning through the whole operation period is highly recommended to devote more machine time to final IP tuning.

VI. CONCLUSION

In conclusion, the ultralow β^* optics has been tuned at ATF2 to demonstrate the operability of a FFS with the CLIC chromaticity level. Following a complex tuning procedure, a tens of nanometers vertical beam size has been verified through tuning simulation and validated experimentally. In the simulation, a multishot beam size of 38.3 ± 5.6 nm accompanied with an IP vertical position jitter of about 20 nm has been predicted, in the presence of realistic multipoles and static and dynamic machine errors. The tuning experiment, conducted in June 2019, has demonstrated the capability of achieving over long periods a vertical beam size below 60 nm. Moreover, a minimum beam size of 50.1 ± 0.6 nm has been obtained during the tuning process. These results are comparable to the performances achieved in the 10×1 and half-β^* optics and represent an important step toward the ultimate 23 nm design beam size.

The discrepancy between the measured and predicted vertical beam sizes is interpreted as the beam size growth engendered by multipolar errors, beam jitters and wakefields, and the IPBSM diagnostic errors. A quantitative analysis has been established to evaluate the contributions from these systematic effects regarding the realistic beam parameters, which further permits an offline correction of the measured beam sizes. Single-shot zero-current beam sizes of 35.5 and 30.7 nm, consistent with the simulations, are predicted for the achieved 50.1 and 41.1 nm minimum beam sizes in the ultralow β^* and 10×1 optics, respectively. To observe a beam size closer to the design value, the nanometer-level beam stabilization techniques, the minimization of the wakefield effects, and the improvement of the IPBSM will be of great importance. For the near future, consecutive tuning with an optimal octupole configuration and the upstream beam stabilization have been proposed.

ACKNOWLEDGMENTS

The authors express their gratitude to the ATF2 Collaboration and the staff of ATF. We also thank P. Bambade, G. White, D. R. Bett, N. Blaskovic Kraljevic, C. Gohil, A. Jeremie, and A. Latina for many helpful discussions and help in simulations and experiments.

[1] M. Aicheler, P. Burrows, M. Draper, T. Garvey, P. Lebrun, K. Peach *et al.*, CLIC conceptual design report, 2014.

[2] ILC Global Design Effort, ILC technical design report, 2013.

[3] P. Bambade, T. Barklow, T. Behnke, M. Berggren, J. Brau, and P. Burrows, The International Linear Collider: A global project, arXiv:1903.01629.

[4] P. Raimondi and A. Seryi, Novel Final Focus Design for Future Linear Colliders, Phys. Rev. Lett. **86**, 3779 (2001).

[5] R. Tomás, Overview of the Compact Linear Collider, Phys. Rev. Accel. Beams **13**, 014801 (2010).

[6] F. Plassard, A. Latina, E. Marin, R. Tomás, and P. Bambade, Quadrupole-free detector optics design for the Compact Linear Collider final focus system at 3 TeV, Phys. Rev. Accel. Beams **21**, 011002 (2018).

[7] B. Grishanov, P. Logachev, F. Podgorny, V. Telnov, D. Angal-Kalinin, R. Appleby *et al.*, ATF2 proposal, 2005.

[8] P. Bambade, M. A. Pons, J. Amann, D. Angal-Kalinin, R. Apsimon, S. Araki *et al.*, Present status and first results of the final focus beam line at the KEK Accelerator Test Facility, Phys. Rev. Accel. Beams **13**, 042801 (2010).

[9] G. White, ATF2 optics design, ICFA Beam Dyn. Newslett. **61**, 26 (2013), https://inspirehep.net/literature/1281129.

[10] G. White, R. Ainsworth, T. Akagi, J. Alabau-Gonzalvo, D. Angal-Kalinin, S. Araki *et al.*, Experimental Validation of a Novel Compact Focusing Scheme for Future Energy-Frontier Linear Lepton Colliders, Phys. Rev. Lett. **112**, 034802 (2014).

[11] R. Tomás, H. Braun, J. Delahaye, E. Marin, D. Schulte, F. Zimmermann *et al.*, ATF2 ultra-low β_y^* proposal, in *Proceedings of the 23rd Particle Accelerator Conference, Vancouver, Canada, 2009* (IEEE, Piscataway, NJ, 2009), pp. 1–3.

[12] E. Marin, R. Tomás, B. Parker, P. Bambade, S. Kuroda, T. Okugi *et al.*, Scenarios for the ATF2 ultra-low betas proposal, in *Proceedings of the International Particle Accelerator Conference, Kyoto, Japan* (ICR, Kyoto, 2010), pp. 4554–4556.

[13] E. Marin, R. Tomás, P. Bambade, K. Kubo, T. Okugi, T. Tauchi *et al.*, Design and high order optimization of the Accelerator Test Facility lattices, Phys. Rev. Accel. Beams **17**, 021002 (2014).

[14] M. Patecki, A. Aloev, D. R. Bett, M. Modena, R. Tomás, E. Marin, G. White *et al.*, Towards ultra-low β^* in ATF2, in *Proceedings of the 6th International Particle Accelerator Conference (IPAC 2015): Richmond, VA, 2015* (JACoW, Geneva, 2015), pp. 38–41.

[15] M. Patecki, D. Bett, E. Marin, F. Plassard, R. Tomás, K. Kubo *et al.*, Probing half β_y^* optics in the Accelerator Test Facility 2, Phys. Rev. Accel. Beams **19**, 101001 (2016).

[16] F. Plassard, Optics optimization of longer L* beam delivery system designs for CLIC and tuning of the ATF2 final focus system at ultra-low β^* using octupoles, Ph.D. thesis, Universite Paris-Saclay, 2018.

[17] T. Okugi, Achievement of small beam size at ATF2 beamline, in *Proceedings of the 28th Linear Accelerator Conference, LINAC16, East Lansing, MI, 2016* (JACoW, Geneva, 2016), pp. 27–31.

[18] M. Woodley, ATF2 measurement: Extraction tuning and matching, ICFA Beam Dyn. Newslett. **61**, 36 (2013), https://inspirehep.net/literature/1281133.

[19] A. Faus-Golfe, J. Navarro, N. F. Martinez, J. R. Lopez, and J. G. Navarro, Emittance reconstruction from measured

beam sizes in ATF2 and perspectives for ILC, Nucl. Instrum. Methods Phys. Res., Sect. A **819**, 122 (2016).

[20] R. J. Apsimon, D. R. Bett, N. B. Kraljevic, P. N. Burrows, G. B. Christian, C. I. Clarke *et al.*, Design and performance of a high resolution, low latency stripline beam position monitor system, Phys. Rev. Accel. Beams **18**, 032803 (2015).

[21] R. J. Apsimon, D. R. Bett, N. B. Kraljevic, R. M. Bodenstein, T. Bromwich, P. N. Burrows *et al.*, Design and operation of a prototype interaction point beam collision feedback system for the International Linear Collider, Phys. Rev. Accel. Beams **21**, 122802 (2018).

[22] T. Okugi, S. Araki, P. Bambade, K. Kubo, S. Kurado, M. Masuzawa *et al.*, Linear and second order optics corrections for the KEK Accelerator Test Facility final focus beam line, Phys. Rev. Accel. Beams **17**, 023501 (2014).

[23] J. Snuverink, R. Ainsworth, S. T. Boogert, F. J. Cullinan, A. Lyapin, Y. I. Kim *et al.*, Measurements and simulations of wakefields at the Accelerator Test Facility 2, Phys. Rev. Accel. Beams **19**, 091002 (2016).

[24] F. Hinode *et al.*, ATF design and study report, KEK Internal Report No. KEK-INT-95-4, 1995.

[25] K. Kubo, M. Akemoto, S. Anderson, T. Aoki, S. Araki, K. Bane *et al.*, Extremely Low Vertical-Emittance Beam in the Accelerator Test Facility at KEK, Phys. Rev. Lett. **88**, 194801 (2002).

[26] K. Honda, K. Kubo, S. Anderson, S. Araki, K. Bane, A. Brachmann *et al.*, Achievement of Ultralow Emittance Beam in the Accelerator Test Facility Damping Ring, Phys. Rev. Lett. **92**, 054802 (2004).

[27] T. Shintake, Proposal of a nanometer beam size monitor for $e+e-$ linear colliders, Nucl. Instrum. Methods Phys. Res., Sect. A **311**, 453 (1992).

[28] P. Tenenbaum and T. Shintake, Measurement of small electron-beam spots, Annu. Rev. Nucl. Part. Sci. **49**, 125 (1999).

[29] T. Suehara, M. Oroku, T. Yamanaka, H. Yoda, T. Nakamura, Y. Kamiya *et al.*, A nanometer beam size monitor for ATF2, Nucl. Instrum. Methods Phys. Res., Sect. A **616**, 1 (2010).

[30] J. Yan, Y. Yamaguchi, Y. Kamiya, S. Komamiya, M. Oroku, T. Okugi, N. Terunuma, K. Kubo, T. Tauchi, and J. Urakawa, Measurement of nanometer electron beam sizes with laser interference using Shintake monitor, Nucl. Instrum. Methods Phys. Res., Sect. A **740**, 131 (2014).

[31] J. Yan, Precise measurement of nanometer scale electron beam sizes using laser interference by Shintake monitor, Ph.D. Thesis, Tokyo University, 2015.

[32] T. Yasui, Experimental study of Shintake electron beamsize monitor at ATF2, Master thesis, Tokyo University, 2018.

[33] J. Pfingstner, H. Garcia-Morales, A. Latina, M. Patecki, D. Schulte, and R. Tomás, Localisation of beam offset jitter sources at ATF2, in *Proceedings of the 5th International Particle Accelerator (IPAC2014), Dresden, Germany, 2014* (JACoW, Geneva, 2014), pp. 1049–1051.

[34] T. Naito and T. Okugi (private communication).

[35] B. Bolzon, N. Geffroy, A. Jeremie, M. Oroku, T. Yamanaka, Y. Kamiya *et al.*, Linear collider final doublet considerations: ATF2 vibration measurements, in *Proceedings of the 23rd Particle Accelerator Conference, Vancouver, Canada, 2009* (IEEE, Piscataway, NJ, 2009), pp. 3654–3656.

[36] B. Bolzon, A. Jeremie, A. Seryi, P. Bambade, and Y. Renier, Linear collider test facility: ATF2 final focus active stabilisation pertinence, in *Proceedings of the 23rd Particle Accelerator Conference, Vancouver, Canada, 2009* (IEEE, Piscataway, NJ, 2009), pp. 3651–3563.

[37] J. Pfingstner, K. Artoos, C. Charrondiere, S. Janssens, M. Patecki, Y. Renier *et al.*, Mitigation of ground motion effects in linear accelerators via feed-forward control, Phys. Rev. Accel. Beams **17**, 122801 (2014).

[38] A. Sery and O. Napoly, Influence of ground motion on the time evolution of beams in linear colliders, Phys. Rev. E **53**, 5323 (1996).

[39] J. Pfingstner, Mitigation of ground motion effects via feedback systems in the Compact Linear Collider, Ph.D. Thesis, Vienna University of Technology, 2013.

[40] V. Shiltsev, Review of observations of ground diffusion in space and in time and fractal model of ground motion, Phys. Rev. Accel. Beams **13**, 094801 (2010).

[41] SAD is a computer program for accelerator design; see http://acc-physics.kek.jp/SAD/.

[42] A. Pastushenko, Nonlinear optimization of the ultra-low beta* optics, in *Proceedings of the International Workshop on Future Linear Collider, 2019* (to be published).

[43] D. R. Bett, N. B. Kraljevic, R. M. Bodenstein, T. Bromwich, P. N. Burrows, G. B. Christian *et al.*, Performance of nanometre-level resolution cavity beam position monitors at ATF2, in *Proceedings of the 9th International Particle Accelerator Conference (IPAC2018), Vancouver, 2018* (JACoW, Geneva, 2018), pp. 1212–1214.

[44] D. R. Bett, C. Charrondiere, M. Patecki, J. Pfingstner, D. Schulte, R. Tomás *et al.*, Compensation of orbit distortion due to quadrupole motion using feed-forward control at KEK ATF, Nucl. Instrum. Methods Phys. Res., Sect. A **895**, 10 (2018).

[45] T. Okugi, Summary of status and study plan for ATF2 intensity dependence measurement, in *Proceedings of the International Workshop on Future Linear Collider, 2018* (to be published).

[46] P. Korysko, A. Latina, A. Faus-Golfe, P. N. Burrows, K. Kubo, T. Okugi *et al.*, Studies of wakefield effects on beam propagation at the KEK Accelerator Test Facility (ATF2) and implications for the International Linear Collider (to be published).